

Regular Article

GeoCLR: Georeference Contrastive Learning for Efficient Seafloor Image Interpretation

Takaki Yamada¹, Adam Prügel-Bennett¹, Stefan B. Williams², Oscar Pizarro^{2,3}
and Blair Thornton^{1,4}

¹Centre for In Situ and Remote Intelligent Sensing, University of Southampton, Southampton SO16 7QF, U.K.

²Australian Centre for Field Robotics, The University of Sydney, NSW 2006, Australia

³Department of Marine Technology, Norwegian University of Science and Technology, 7491 Trondheim, Norway

⁴Institute of Industrial Science, The University of Tokyo, 4-6-1 Komaba Meguro-ku, Tokyo 153-8505, Japan

Abstract: This paper describes georeference contrastive learning of visual representation (GeoCLR) for efficient training of deep-learning convolutional neural networks (CNNs). The method leverages georeference information by generating a similar image pair using images taken of nearby locations, and contrasting these with an image pair that is far apart. The underlying assumption is that images gathered within a close distance are more likely to have similar visual appearance, where this can be reasonably satisfied in seafloor robotic imaging applications where image footprints are limited to edge lengths of a few meters and are taken so that they overlap along a vehicle's trajectory, whereas seafloor substrates and habitats have patch sizes that are far larger. A key advantage of this method is that it is self-supervised and does not require any human input for CNN training. The method is computationally efficient, where results can be generated between dives during multi-day autonomous underwater vehicle (AUV) missions using computational resources that would be accessible during most oceanic field trials. We apply GeoCLR to habitat classification on a dataset that consists of ~86,000 images gathered using an AUV. We demonstrate how the latent representations generated by GeoCLR can be used to efficiently guide human annotation efforts, where the semi-supervised framework improves classification accuracy by an average of 10.2% compared to the state-of-the-art SimCLR using the same CNN and equivalent number of human annotations for training.

Keywords: computer vision, environmental monitoring, learning, marine robotics, underwater robotics

Received: 15 April 2021; revised: 20 February 2022; accepted: 20 April 2022; published: 9 June 2022.

Correspondence: Takaki Yamada, Centre for In Situ and Remote Intelligent Sensing, University of Southampton, Southampton SO16 7QF, U.K., Email: T.Yamada@soton.ac.uk

This is an open-access article distributed under the terms of the Creative Commons Attribution License, which permits unrestricted use, distribution, and reproduction in any medium, provided the original work is properly cited.

Copyright © 2022 Yamada, Prügel-Bennett, Williams, Pizarro and Thornton

DOI: <https://doi.org/10.55417/fr.2022037>

1. Introduction

Robotic imaging surveys can enable regional-scale understanding of seafloor substrate and habitat distributions. Since visual images are limited to edge lengths of a few meters in water due to the strong attenuation of light, multiple overlapping georeferenced images need to be gathered to describe larger-scale patterns that exist on the seafloor. Camera-equipped autonomous underwater vehicles (AUVs) achieve this by gathering tens of thousands of images during their dives at close and near-constant altitudes, with most AUV expeditions lasting many weeks and consisting of several deployments. However, taking advantage of the growing repositories of seafloor images is a challenge because our ability to interpret images cannot keep up with the influx of data.

Modern machine learning techniques have demonstrated robust, automated image interpretation. Much of the progress in this area has been driven by the availability of generic datasets consisting of over a million human-labeled images to supervise the training of deep-learning convolutional neural networks (CNNs). In domains with high learning transferability, this allows deep learning to be used in applications where the large amount of human effort required to generate labeled training data would be unjustified. However, the appearance of an underwater image is highly sensitive to the environment (e.g., seawater attenuation properties and turbidity), observation variables (e.g., range to target), and hardware choices (e.g., lighting and camera configurations), and these factors limit transferability of learning across datasets. This has so far limited large-scale generic training datasets from being developed in this domain, and even if these were developed, it is still an open question as to whether these would be as effective as those used in terrestrial applications.

To address this issue, we investigate self-supervision techniques for deep-learning CNNs. Self-supervision is a subset of unsupervised learning, which generates optimized feature descriptors without using human annotations. Self-supervision aims to improve the quality of the image representation by using additional non-image- or image-derived data that can be automatically associated with each image to constrain learning. A key advantage of these methods is that they can generate low-dimensional feature vectors on a per dataset basis, making them effective in domains where there is limited transferability of learning across datasets. Once the representations are obtained, various machine learning techniques such as clustering, content retrieval, and few-shot learning can be efficiently applied. Contrastive learning is a form of self-supervision that has demonstrated robust performance gains across many application areas in the image representation learning domain (Chen et al., 2020; Jing and Tian, 2021; Le-Khac et al., 2020). It works by giving similar and dissimilar image pairs to a CNN, optimizing the representation that gets generated by mapping similar image pairs within a close distance in the latent representation space and dissimilar image pairs so that they are separated in this space. To ensure images are similar without relying on human input, most contrastive learning techniques use data augmentation, i.e., applying random transformation to the same image to obtain similar but not identical pairs of images. In this work, we develop a novel method of georeference enhanced contrastive learning for image representation (GeoCLR), which leverages the 3D location information attached to each image to identify similar pairs of images in the target dataset, making the assumption that physically close images are more likely to be similar in appearance than images taken at a larger spatial interval. This assumption is reasonable for the application considered in this work since AUV imagery is taken at close, often overlapping, spatial intervals, and when describing substrates and habitats, the features of interest span or recur over spatial scales larger than the footprint of an individual image frame.

The contributions of this work are as follows:

- Development of GeoCLR, a novel contrastive representation learning technique for georeferenced seafloor imagery, utilizing an assumption that a pair of images taken physically close to each other are more likely to have similar appearance than a random pair when identifying similar and dissimilar image pairs in a dataset;
- Development of an efficient method to use self-supervised learning outputs to guide human labeling effort to improve the accuracy of low-shot classification; and

- Experimental verification of the proposed method’s effectiveness through comparison with current state-of-the-art transfer learning and augmentation-based contrastive learning, or SimCLR, techniques using a seafloor image dataset consisting of ~86,000 AUV images gathered over 12 dives with over ~5,000 human labels.

2. Background

2.1. Representation Learning for Seafloor Imagery

Visual images of the seafloor contain useful information for mapping substrate and habitat distribution. However, the high dimensionality and redundant information in raw images is a challenge for classification. Therefore, most algorithmic interpretations first convert images to lower-dimensional representations, or feature spaces, that can be more efficiently analyzed. Several types of feature descriptor have been investigated for seafloor image representations (Beijbom et al., 2012; Bewley et al., 2015; Kaeli and Singh, 2015; Neettiyath et al., 2021; Rao et al., 2017; Steinberg et al., 2011). In Beijbom et al. (2012) and Neettiyath et al. (2021), color descriptors are designed to target known targets of scientific interest, such as corals (Beijbom et al., 2012) and mineral deposits (Neettiyath et al., 2021). Generic feature descriptors such as local binary patterns (LBPs) (Ojala et al., 2002) and sparse coding spatial pyramid matching (ScSPM) (Yang et al., 2009) have also been applied to capture multi-scale spatially invariant patterns in seafloor images (Bewley et al., 2015; Rao et al., 2017). In Kaeli and Singh (2015), histograms of oriented gradients from image keypoints are applied for clustering and anomaly detection. These approaches share common steps of selecting effective descriptors and parameter tuning, or feature engineering, that can be time consuming and require knowledge of how targets of interest are expected to appear in the images.

CNNs avoid the need for feature engineering by learning the representations needed to describe the datasets they are trained on. In supervised learning, this is achieved using human-annotated examples in a training dataset, where the latent representations and class boundaries to best describe the patterns of interest are simultaneously optimized. In Mahmood et al. (2018), the deep-learning CNN ResNet (He et al., 2016) is trained to classify nine different types of coral in a seafloor image dataset, demonstrating higher classification resolution and accuracy than traditional feature engineering methods. However, the need for large volumes of annotated images limits wide-scale use in marine applications as generic training methods and datasets do not currently exist in this domain.

2.2. Self-Supervised Learning for Seafloor Imagery

An alternative approach to train CNNs is self-supervised learning using properties of the data that can be utilized without the need for direct human supervision. Unlike state-of-the-art supervised training methods such as transfer learning, where CNNs are pre-trained with large annotated datasets such as ImageNet (Deng et al., 2009), self-supervised methods train CNNs on the target dataset itself and so are effective in domains where there is a limited transferability of learning between the target dataset and those available for pre-training. In Yamada et al. (2021b), a deep-learning convolutional autoencoder based on AlexNet (Krizhevsky et al., 2012) is used for representation learning of seafloor images. Autoencoders consist of an encoder and decoder pair, where the encoder maps the original data into low-dimensional latent representations. Next, the decoder reconstructs the original data from the low-dimensional latent representation, where both the encoder and decoder networks are optimized to make the reconstructed data as similar to the original input data as possible. This dimensional reduction attempts to remove redundant information in the raw inputs, retaining only the most important information in compact latent representations at the encoder output. In Yamada et al. (2021b), the authors developed a location guided autoencoder (LGA) that uses horizontal location information to regularize learning by using the assumption that images captured at nearby locations are more likely to look similar than

images that are far apart since seafloor habitats and substrates exhibit patterns larger than the footprint of a single image frame. The method significantly outperformed standard convolutional autoencoders without location regularization, achieving a factor of 2 improvement in normalized mutual information when applied to clustering and content-based retrieval tasks. In Yamada et al. (2021a), the LGA is extended to utilize other types of metadata, such as depth information, where the continuity in measurements has potential correlation with image appearance, where it was demonstrated that these terms can be included without risk of performance degradation through the design of a robust regularization process.

2.3. Contrastive Learning Concepts for Image Representation

The recent development of contrastive learning concepts has demonstrated significant performance gains in self-supervised representation learning (Jing and Tian, 2021; Le-Khac et al., 2020). The main idea behind contrastive concepts is to simultaneously provide similar and dissimilar image pairs during training, where similar pairs are mapped close to each other in the representation space, and dissimilar pairs are mapped far apart. These concepts require a binary prior that describes whether the image pairs provided during training are expected to be similar or not.

In Chen et al. (2020), a method to generate similar and dissimilar pairs without any direct human input is developed using data augmentation. The proposed SimCLR applies random data augmentations to artificially generate similar image pairs, which are then contrasted with dissimilar pairs where different images are used. The method demonstrated significant gains in performance compared to supervised training using the transfer learning approach (Tan et al., 2018).

3. Contrastive Representation Learning Using Georeference Information

The use of location information to regularize autoencoder training can enhance the performance of seafloor image representation Yamada et al. (2021a,b). Here, we investigate whether georeference information can also be used to improve the latent representations generated in contrastive learning (Chen et al., 2020). Unlike the modified autoencoder loss functions used in our previous work where location information can be used to loosely regularize learning, the binary similarity condition that is imposed in contrastive learning forces a much stronger constraint on the latent representations that get generated. In order to validate this similarity assumption, we take advantage of the fact that AUVs capture images that often overlap and have footprints that are generally smaller than the patch size of habitats and substrates on the seafloor.

The following subsections give an overview of state-of-the-art modern contrastive learning approaches such as SimCLR (Chen et al., 2020), and introduce a novel GeoCLR method for efficient representation of spatially contiguous georeferenced imagery.

3.1. SimCLR

SimCLR learns representations by maximizing agreement between differently augmented images generated from the same original image. The learning framework, illustrated in Figure 1a, consists of four parts: data augmentation, base encoder $f(\cdot)$, projection head $g(\cdot)$, and a contrastive loss function. Data augmentation transforms each image \mathbf{x} in the target dataset randomly to artificially generate two correlated images, $\tilde{\mathbf{x}}_i$ and $\tilde{\mathbf{x}}_j$, where random cropping, color distortions, and Gaussian blur augmentations are applied in this order. The base encoder $f(\cdot)$ is a CNN that extracts representation vectors from the augmented images. The method allows any CNN to be used for $f(\cdot)$, where Chen et al. (2020) found this approach to be most effective on deeper and wider ResNet (He et al., 2016) architectures. $\mathbf{h}_i \in \mathbb{R}^d$ is a feature vector extracted from $\tilde{\mathbf{x}}_i$ by the base encoder ($\mathbf{h}_i = f(\tilde{\mathbf{x}}_i)$). The projection head $g(\cdot)$ is a two-layer multilayer perceptron (MLP) to obtain $\mathbf{z}_i \in \mathbb{R}^{d'}$ ($\mathbf{z}_i = g(\mathbf{h}_i)$). The dimension d' of the MLP output is smaller than the dimension d of the base encoder since the contrastive losses defined in lower-dimensional spaces are more efficient

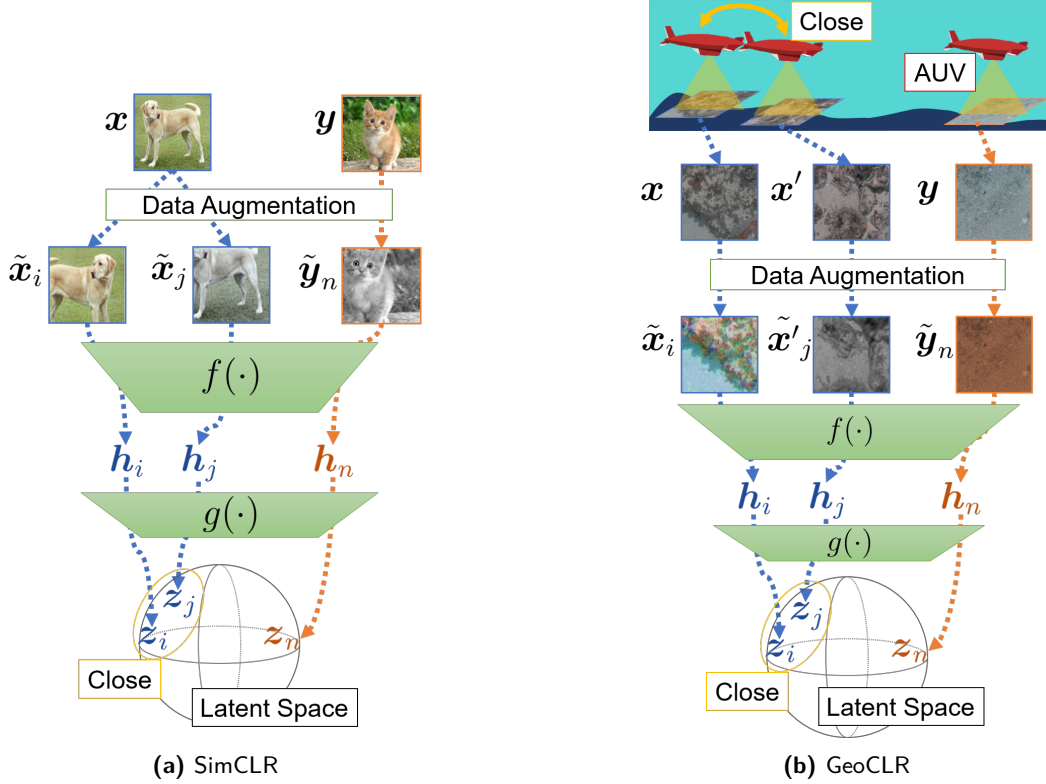


Figure 1. Overview of SimCLR and the proposed GeoCLR. The two methods apply different conditions to generate similar pairs of images to implement contrastive learning. (a) In SimCLR, similar image pairs $[\tilde{x}_i, \tilde{x}_j]$ are generated by applying different random augmentations to the same image x . (b) The proposed GeoCLR generates similar pairs $[\tilde{x}_i, \tilde{x}'_j]$ using different images that were taken from physically nearby locations, x and x' . The large range of variability captured in the generated similar pairs allows for robust CNN training.

for representation learning. A minibatch of N original images is taken into consideration at each iteration, so $2N$ augmented images including N similar pairs are sampled. For a similar pair, other $2(N - 1)$ augmented images (\tilde{y}_n in Figure 1a) can be regarded as dissimilar examples within the minibatch. The normalized temperature-scaled cross entropy loss function (*NT-Xent*) (Sohn, 2016; Wu et al., 2018; van den Oord et al., 2018) between the similar pair \tilde{x}_i and \tilde{x}_j is defined as

$$\ell_{i,j} = -\log \frac{\exp(\text{sim}(z_i, z_j)/\tau)}{\sum_{k=1}^{2N} \mathbb{1}_{[k \neq i]} \exp(\text{sim}(z_i, z_k)/\tau)}, \quad (1)$$

where $\text{sim}(\cdot)$ denotes cosine similarity, $\mathbb{1}_{[k \neq i]} \in \{0, 1\}$ is the indicator function which is 1 if $k \neq i$, and τ is the temperature parameter. The total minibatch loss can be written as

$$\mathcal{L} = \frac{1}{2N} \sum_{k=1}^N [\ell(2k - 1, 2k) + \ell(2k, 2k - 1)]. \quad (2)$$

The parameters of the base encoder $f(\cdot)$ and the projection head $g(\cdot)$ are updated by a stochastic gradient descent (SGD) optimizer with linear rate scaling (Goyal et al., 2017).

SimCLR can efficiently train CNNs using large unannotated image datasets, where the latent representations derived from the original images x were shown to outperform other state-of-the-art methods in the benchmark classification tasks. It was further shown that fine-tuning of SimCLR trained CNNs can achieve more accurate classification with two orders of magnitude fewer labels than conventional supervised training methods.

3.2. GeoCLR

A limitation of SimCLR is that the variety of possible image appearances is limited by the types of augmentation used, and only features intrinsic to each image can be efficiently extracted. However, when applied to practical semantic interpretation, we are typically interested in correlating images that show a greater degree of variability than can be described by algorithmic augmentation alone. We predict that the performance of downstream interpretation tasks will benefit if a greater variety of appearances can be integrated into the similar pairs during CNN training. The GeoCLR method proposed in this paper allows great variability to be introduced into the similar image pairs by utilizing the georeference information associated with each image. We argue that the level of variability between images taken nearby will exhibit a level of variability that is more representative of that seen across similar habitats or substrates than augmentation alone.

Figure 1b shows the overview of GeoCLR. In GeoCLR, each similar image pair $[\tilde{\mathbf{x}}_i, \tilde{\mathbf{x}}'_j]$ is generated from two different images, where $\tilde{\mathbf{x}}_i$ and $\tilde{\mathbf{x}}'_j$ are generated from \mathbf{x}' , which is a different image than \mathbf{x} but is taken of a physically nearby location. For each image \mathbf{x} captured at the 3D georeference of $(g_{east}, g_{north}, g_{depth})$, \mathbf{x}' is randomly selected at each iteration from the images which satisfy the following criteria:

$$\sqrt{(g'_{east} - g_{east})^2 + (g'_{north} - g_{north})^2 + \lambda(g'_{depth} - g_{depth})^2} \leq r, \quad (3)$$

where $(g'_{east}, g'_{north}, g'_{depth})$ is the 3D georeference of \mathbf{x}' , and λ is the scaling factor for depth direction. Introducing $\lambda > 1$ allows the depth difference between images to be weighted so that the nearby images with large depth gap are not selected, where values of $\lambda < 1$ tend to ignore differences in depth. This flexibility is introduced because the relative impact that depth has on image appearance can vary across different applications, where for example shallow water applications typically have a stronger correlation due to the variable influence of sunlight reaching the seafloor than deep-sea applications. To identify an image pair, the distance r needs to be larger than the distance between adjacent images taking into account variability in the acquisition interval, and smaller than the patch size of substrates and habitats so that paired images are likely to be similar in appearance. In practice, a small value is advantageous since the similarity assumption is likely to be violated near patch boundaries as r increases. The lower limit for r should also be conservatively set since restricting pairs to only its nearest neighbor means that the same pairing is more likely to be selected multiple times during training, which does not generate any additional information compared to the original SimCLR.

Once \mathbf{x}' is selected, the same types of random data augmentation used in SimCLR are applied to each image to obtain the similar pair $[\tilde{\mathbf{x}}_i, \tilde{\mathbf{x}}'_j]$.

4. Experiment

The proposed GeoCLR is applied to a dataset consisting of 86,772 georeferenced seafloor images obtained off the coast of Tasmania. The CNN is first trained on all images in the dataset to generate latent representations. Next, classification tasks are given to the trained CNN and the extracted features by the CNN, so that the performance can be evaluated based on classification accuracy. A variety of methods are used to train these classifiers, including the use of the latent representations to guide human annotation effort for efficient low-shot semi-supervised learning. The performance of the proposed GeoCLR is evaluated through comparison with SimCLR and transfer learning under the equivalent conditions.

4.1. Dataset

The Tasmania dataset used for evaluating the proposed GeoCLR (Williams et al., 2012) is shown in Figure 2 and described in Table 1. The dataset consists of 86,772 seafloor images taken by the Australian Centre for Field Robotics' Sirius AUV from a target altitude of 2 m. The dataset contains

Table 1. Tasmania dataset description

Vehicle	Sirius AUV
Camera Resolution	1,360 × 1,024
Camera FoV	42 × 34 deg
Frame Rate	1 Hz
Year	2008
Location	East Coast of Tasmania, Australia
Coordinate	43.08°S, 147.97°E
Depth	28–96 m
Altitude	1.0–3.0 m
Ave. Velocity	0.5 m/s
No. of Images	86,772
No. of Annotations	5,369
No. of Classes	6 (see Figure 3)
No. of Dives	12

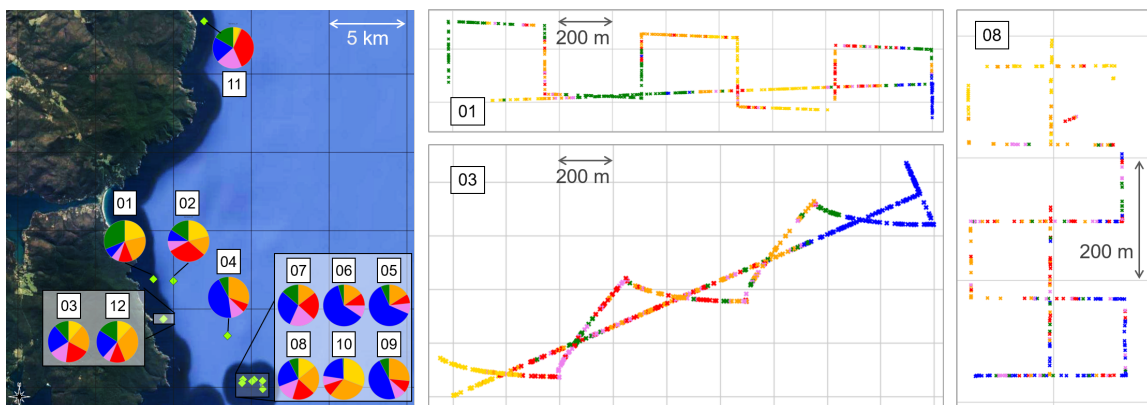


Figure 2. Map of the surveyed area (east coast of Tasmania). The images were gathered through 12 AUV deployments. The start points of each deployment are shown as green dots. The pie charts show the class distributions according to human expert annotations. The same color scheme is used as in Figure 3, which shows example images of each class. The survey paths of dives 01, 03, and 08 are shown with the human-annotated class distributions on the right.

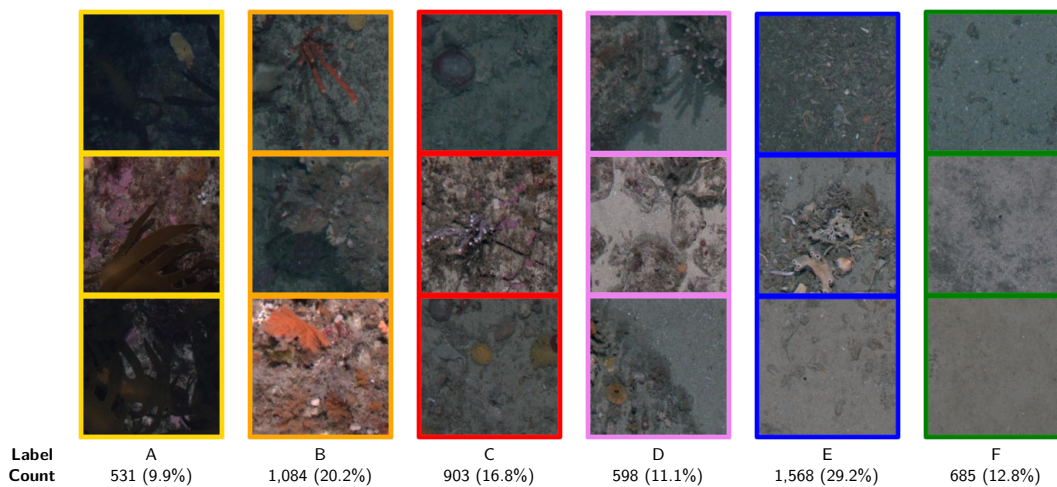


Figure 3. Class example images together with the number of expert human annotations in each class: A - kelp, B - high relief reef, C - low relief reef, D - reef and sand, E - screw shell rubble, F - sand.

habitat and substrate distributions as shown in Figure 3, including kelp (A), a registered essential ocean variable, and rocky reefs (B, C, D), which can form habitats for various conservation targets such as coral and sponges (Moltmann et al., 2019). 5,369 randomly selected images are annotated by human experts into six classes, as shown in Figure 3. 50 images randomly selected from each of 6 classes (total of 300 images) are used for validation and $M=[40, 100, 200, 400, 1000]$ images selected from the remaining 5,069 annotated images are used for training, following the evaluation protocol described in Section 4.3. The georeference information of each image is determined based on the stereo simultaneous localization and mapping (SLAM) pipeline described in Mahon et al. (2008) and Johnson-Roberson et al. (2010). The original resolution of the images is $1,360 \times 1,024$, where the average distance between adjacent images is approximately 0.5 m, so some images partly overlap each other. Prior to analysis, each image in the dataset is re-scaled to a resolution of 2 mm/pixel based on the imaging altitude. Randomly cropped 224×224 regions of the images are used for training, where validation is performed on the the same sized regions cropped from the center of the images.

4.2. GeoCLR Training Configuration

GeoCLR can be used to train any type of CNN. Here we use the well established ResNet18 (He et al., 2016) for benchmarking. The latent representation \mathbf{h} and \mathbf{z} dimensions are set to $d = 512$ and $d' = 128$, respectively. A minibatch size of $N = 256$, learning rate of 3.0×10^{-4} , weight decay of 1.0×10^{-4} , and temperature $\tau = 0.07$ in equation 1 was used for all experiments. The threshold of closeness and depth scaling factor in equation 3 were set to $r = 1.0$ m and $\lambda = 1.0$, respectively. The value for r is conservative compared to the expected substrate and habitat patch size in the surveyed region, and was chosen to yield two to four nearby images based on the average distance between images (see Table 1). This minimizes the probability of nonsimilar image pairs being selected near patch boundaries and the likelihood of duplicate pairs being selected during training. Results on the sensitivity of learning performance to a range of $r = 0, 1.0, 3.0, 5.0, 10.0$ m included in the Appendix demonstrate this trend, with no benefit seen beyond $r = 3.0$ m for the dataset analyzed in this paper. As expected, a small value of r is advantageous, with the limit of sufficiently nearby images being unavailable if it is set too small. The mean range between best and worst performing conditions is 3.7% for equivalent M and λ numbers. The value of λ was chosen to evenly treat horizontal and vertical displacement between images. Analysis in the Appendix for $\lambda = 0, 0.5, 1.0, 3.0, 5.0, 10.0$ shows that the performance sensitivity is small. The mean range between best and worst performing conditions is 1.7% for equivalent M and r numbers. The sensitivity and optimum value for λ is likely to be dataset dependent, and more significant in datasets that have high rugosity.

Other than the method for generating similar image pairs, identical parameters were used for GeoCLR and SimCLR to allow for comparison. Both methods are trained on all 86,772 images in the dataset. We also benchmark the performance of the proposed method against conventional supervised transfer learning using ResNet18 that was pre-trained on ImageNet.

Though deeper CNN architectures, larger minibatch sizes, and epoch are known to provide accuracy gains for SimCLR, these above parameters are set considering the computational power that can be reasonably deployed in the field, where access to high-performance computer networks is limited. The workstation used for experiments in this paper used a single NVIDIA TITAN RTX with 24 GB VRAM. The GeoCLR training and fine tuning with pseudo-labeling carried out in this work each took approximately a day (26 hours for GeoCLR training and a few minutes for fine-tuning) for the dataset of $\sim 86,000$ images gathered in 24 hours of bottom time over multiple AUV dives. This indicates that the results could be made available in timeframes relevant to assist planning and interpretation between dives during multi-day field expeditions.

4.3. Evaluation Protocol

CNNs trained using three different approaches (ImageNet, SimCLR, GeoCLR) are evaluated following the protocol used by Chen et al. (2020). Once the CNNs are trained, the latent representations

they generated are analyzed using different classifiers; a linear logistic regression, a nonlinear support vector machine (SVM) with a radial basis function (RBF) kernel, and a fine-tuned CNN classifier. The logistic regression and SVM with RBF kernel are both trained on the latent representation space output \mathbf{h} of ResNet18 after CNN training. For fine-tuning, a minibatch size of 256, Adam optimizer with learning rate of 3.0×10^{-4} , and no weight decay were used. The macro averaged f_1 score over six classes determined from the independent validation set is used to compare the classification accuracy of each training method. All experiments are repeated 10 times in each configuration, where the standard deviation (SD) of scores is shown alongside the mean value to describe variability.

We perform experiments to evaluate classification performance using $M=[40, 100, 200, 400, 1000]$ training examples selected using the following sampling strategies:

- *Balanced*: M annotated images are selected so that all classes are equally represented.
- *Random*: M annotated images are randomly selected without any constraint.
- *H-k means*: M annotated images are selected using hierarchical k means to evenly represent different regions of the latent representation space learned through self-supervised training.

Class-balanced training examples can be considered ideal for supervised learning in applications where all classes are of equal importance. However, this requires significant human effort to determine the relevant classes and identify images corresponding to each class, which is not practical for most field survey scenarios. The *random* method is relevant for most survey scenarios, and can make the effort in annotation more manageable in situations where the class distribution in the target dataset is not known. However, the method suffers when the number of images in each class is not balanced; since classes are represented in proportion to their relative abundance, those with small populations tend to exhibit poor performance. The hierarchical k -means clustering (Nister and Stewenius, 2006), or *H-k-means*, method allows for balanced representation of the variety of images present in a dataset without the need for additional human effort, and was shown to be effective for guiding human labeling effort in Yamada et al. (2022). In this method, k -means clustering is first applied to latent representations with $k = m$ to find representative clusters of images in the dataset. An appropriate value for m can be automatically determined for each dataset using the elbow method (Satopaa et al., 2011), where a value of $m = 10$ was found to be appropriate for the dataset used in this experiment. Next, each cluster is further subdivided using k -means clustering where $k = M/m$, to identify images closest to the centroid of each subdivided cluster, which is prioritized for human annotation. If the latent representations describe original images appropriately, the cluster boundaries found in the first k -means clustering are expected to approximate the class boundaries, allowing the class imbalance problem in *random* selection to be eased by selecting the same number of images from each cluster. The second k -means clustering avoids selecting similar samples from within each cluster, so that the full variety of images in the dataset can be represented by a small number of annotations. This *H-k-means* selection was shown to outperform *random* selection when appropriate latent representations are generated (Yamada et al., 2022). The same work also demonstrated the use of pseudo-labels, generated from the predictions of classical classifiers applied to the latent representations, for CNN fine-tuning, which is also examined in this work.

Two sets of experiments are performed. First, we assess the performance of CNNs using the *balanced* selection strategy. Although this is not realistic for practical field scenarios, the results represent the expected upper bound of performances, and allow the fundamental performance of the three latent representation learning strategies (ImageNet, SimCLR, GeoCLR) to be compared. The second set of experiments compares the performance using *random* and *H-k-means*-based selection strategies, including the use of pseudo labeling with linear logistic regression (PL-linear), a nonlinear SVM with RBF (PL-SVM) for CNN fine-tuning. The sampling strategies can both realistically be implemented in field survey scenarios since they do not assume any prior knowledge of the datasets, and the images that require annotation can be rapidly identified in a fully unsupervised manner.

Table 2. CNN training method comparison on class balanced training subset

Config. Label	CNN Training	Classifier	Number of Annotations (M)				
			40	100	200	400	1000
A1	ImageNet	linear	54.9±4.7	61.6±2.8	63.0±2.2	67.5±2.2	67.4±2.1
A2	ImageNet	SVM	47.0±4.9	55.3±4.9	60.2±2.3	66.2±1.1	69.7±1.1
A3	ImageNet	Res18	58.9±2.6	65.5±2.7	68.2±2.5	71.2±1.7	73.8±1.3
B1	SimCLR	linear	62.5±2.7	65.2±2.8	67.1±1.2	69.2±2.2	71.8±1.0
B2	SimCLR	SVM	62.4±2.7	66.9±1.8	69.2±1.8	71.8±1.4	74.1±1.0
B3	SimCLR	Res18	53.4±4.4	61.3±2.2	65.5±2.0	68.9±2.7	72.4±0.9
C1	GeoCLR	linear	63.8±2.9	67.8±2.4	71.4±1.4	72.9±1.8	74.9±1.0
C2	GeoCLR	SVM	61.7±2.5	70.1±2.4	74.5±1.4	75.8±1.4	78.3±1.1
C3	GeoCLR	Res18	53.6±5.3	62.8±2.2	66.2±2.9	69.5±1.9	73.2±1.3

The CNNs are trained using three different methods (supervised learning by ImageNet, SimCLR, and GeoCLR). The latent representations (h) extracted from the M annotated images by each CNN are used for logistic regression classification (linear) and SVM (with RBF) training. Also the CNNs are fine-tuned on the same subsets of images. The M images are selected so that all six classes in the dataset are evenly described. The classifiers are trained 10 times with different random seed, and mean and SD values of f_1 scores (macro averaged) are shown. The best score for each M is shown as bold.

4.4. Result

4.4.1. Class-Balanced Training Evaluation

Table 2 shows the macro averaged f_1 scores of each CNN training and classifier configuration on the class-balanced subsets of the annotated images. The results show that GeoCLR has the best performance for all values of M , with the linear classifier (C1) showing the best performance for $M = 40$, and the SVM classifier (C2) best for all other M values. The latent representations generated using GeoCLR achieves an average 7.4% and 5.2% increase in performance compared to the best performing ImageNet and SimCLR trained configurations.

Among the ImageNet pre-trained CNN (A*), the CNN fine-tuned using M images (A3) achieves the highest accuracy for all M with an average performance gain of 6.6%. This is owed to the capacity of CNNs to simultaneously optimize feature extraction and classification during training. In A1 and A2, the lower level feature extractor optimized on ImageNet is not updated. The inferior performance compared to A3 indicates that the latent representations generated using ImageNet are suboptimal for the seafloor images used in this work, failing to describe their useful distinguishing features.

In contrast, for SimCLR and GeoCLR trained CNNs (B* and C*) the fine-tuned scores for the ResNet18 classifier are lower than the scores of linear and SVM classifiers. This shows that the constraining effect of contrastive learning in SimCLR or GeoCLR training generates highly optimized latent representations. Since conventional fine-tuning does not maintain this constraining effect, it degrades performance, achieving a similar level of accuracy as fine-tuning of ImageNet pre-trained CNN in A3 for larger values of M . This finding is in contrast to the results of [Chen et al. \(2020\)](#), where fine-tuning of CNNs trained using SimCLR significantly outperforms linear classifiers applied to latent representation space for generic terrestrial image datasets analyzed. Possible reasons for the difference in behavior is the relatively high dimensionality of h ($d = 512$) compared to the small number of classes (6) in the dataset considered in this paper, combined with the continuous transition of image appearance across the class boundaries, both of which are different to terrestrial benchmark datasets, which typically have a larger number of classes with discrete boundaries, both of which can make the latent representation more sensitive to the constraining effect of contrastive learning.

Figure 5a shows representative configurations from Table 2. The proposed GeoCLR with a SVM classifier (C2) outperforms all other configurations except for B2 when $M = 40$. Having said this, the best performance for $M = 40$ is achieved by the GeoCLR with a linear classifier (C1) as can be

seen in Table 2. When the CNNs are fine-tuned, transfer learning with ImageNet (A3) outperforms fine-tuned SimCLR and GeoCLR (B3 and C3).

4.4.2. Data Selection Method Comparison

The performance using the *random* and *H-k-means* training data selection strategies, both of which do not need prior human input to understand the datasets, are shown in Table 3 for different values of M .

The different CNN training methods show the same trend as the previous results with *balanced* training data selection (Table 2). When the classifiers are trained on the latent representations, GeoCLR outperforms SimCLR and ImageNet pre-training, achieving average performance gains of 6.3% and 20.0%, respectively, across all M . As previously observed, fine-tuning SimCLR and GeoCLR trained CNNs degrades their performance. However, the pseudo-labeling introduced in E7, E8, F7, and F8 mitigates this effect by using a larger number of images for fine-tuning, which avoids the problem of overfitting that can occur when only a small number of images are used in fine-tuning. This effect is strongest for small values of $M = 40$ and 100, where performance gains of 13.1% and 8.0% are achieved for both GeoCLR and SimCLR compared to equivalent configurations that do not use PL.

Figure 5b shows representative configurations in Table 3. The configurations with the GeoCLR (F*) outperform their counterparts with the SimCLR (E*) except for the case where $M = 40$ where E4 performs better than F4. In general, the use of *H-k-means* improves performance compared to equivalent *random* configurations, achieving performance gains of 13.1% and 5.7%, respectively, for $M = 40$ and 100. Although the gain in performance reduces for larger M , for GeoCLR *H-k-means* selection always improves performance compared to equivalent *random* configurations for all values of M . An important observation is that the proposed GeoCLR achieved the best performance for all values of M for both the *balanced* and *H-k-means* selection strategies.

A comparison between Table 2 and Table 3 shows that GeoCLR with *H-k-means* performs better than with the *balanced* selection strategy for all values of M , with gains of 3.1% and 2.7% for small values of $M = 40$ and 100, and averaging a performance gain of 1.6%.

The results indicate that it is more valuable and informative to provide training data that evenly describe the latent representation space generated during self-supervised training than it is to provide training data that evenly describe the targets that are of final interest to humans. Figure 4 shows the representative images selected by (a) *Balanced*, (b) *Random*, and (c) *H-k-means*

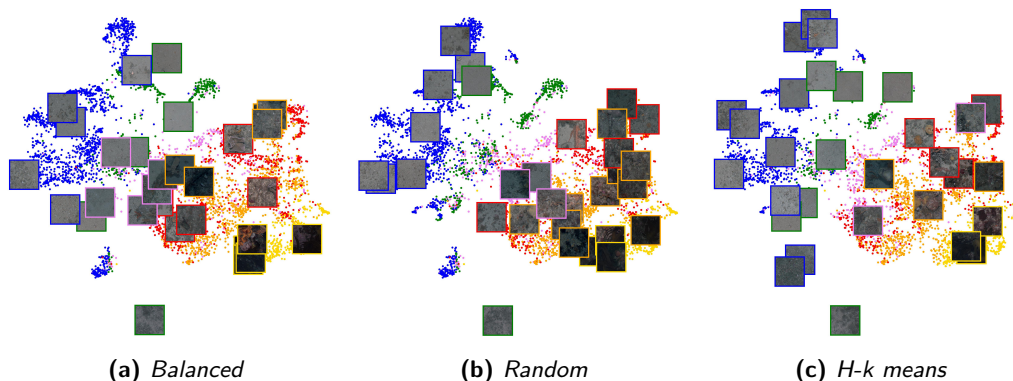


Figure 4. Comparison of training data sampling strategy. $M = 30$ images are selected by (a) *balanced*, (b) *random*, and (c) *H-k-means* strategy. The selected images are shown on t -distributed stochastic neighbor embedding (t -SNE) visualization of latent representations obtained by GeoCLR. While *random* sampling fails to select from the center area, *H-k-means* successfully selects the images in the relatively sparse areas so that a more informative training dataset is gained. Similarly, *balanced* fails to sample regions of the latent space where there are more densely populated regions of the same class. In these situations, class assigned by the classifier will depend on the class of training examples that happen to be nearby. The same color scheme as Figure 3 is applied.

Table 3. Data selection method comparison

Config. Label	CNN Training	Classifier	Data Selection	Number of Annotations (M)				
				40	100	200	400	1000
D1	ImageNet	linear	random	45.4±5.8	57.0±3.2	61.3±2.8	63.3±2.9	67.5±2.2
D2	ImageNet	linear	H- k means	49.5±5.6	58.0±4.7	64.4±3.4	66.5±2.6	68.8±1.8
D3	ImageNet	SVM	random	35.5±4.4	50.2±3.7	58.4±3.3	63.7±1.4	67.9±1.0
D4	ImageNet	SVM	H- k means	43.0±3.4	57.5±2.8	63.7±1.0	67.0±1.4	69.7±1.3
D5	ImageNet	Res18	random	55.5±3.1	63.2±3.2	67.0±2.0	69.7±2.4	72.8±2.3
D6	ImageNet	Res18	H- k means	51.8±5.7	64.1±2.0	67.6±2.7	73.1±1.3	74.1±1.7
D7	ImageNet	Res18	PL-linear	51.9±5.7	62.2±4.5	68.6±1.8	70.9±2.0	71.9±2.3
D8	ImageNet	Res18	PL-SVM	46.4±5.4	58.9±3.4	67.1±1.6	69.9±1.7	72.6±2.1
E1	SimCLR	linear	random	55.0±4.0	63.8±3.0	66.3±2.1	67.7±3.2	71.2±1.1
E2	SimCLR	linear	H- k means	61.9±2.6	66.5±1.6	68.2±1.4	69.3±2.7	69.5±1.9
E3	SimCLR	SVM	random	47.2±5.5	64.5±2.4	68.8±1.6	72.0±2.2	73.5±0.7
E4	SimCLR	SVM	H- k means	58.0±2.0	67.6±1.5	70.9±1.3	71.7±1.8	73.7±1.5
E5	SimCLR	Res18	random	49.5±7.5	60.3±2.2	64.5±2.4	67.7±1.8	71.5±2.3
E6	SimCLR	Res18	H- k means	56.4±3.3	65.2±2.2	66.2±1.7	69.3±2.0	70.1±1.2
E7	SimCLR	Res18	PL-linear	64.3±2.2	68.8±1.4	69.5±1.7	70.5±1.7	72.8±1.3
E8	SimCLR	Res18	PL-SVM	63.1±2.8	69.8±1.8	70.6±1.1	72.7±1.1	72.9±0.8
F1	GeoCLR	linear	random	58.9±5.0	67.8±2.7	70.8±1.7	72.7±2.5	75.1±1.4
F2	GeoCLR	linear	H- k means	65.8±2.9	70.5±1.7	72.8±2.0	73.0±2.1	74.6±2.5
F3	GeoCLR	SVM	random	53.2±5.9	68.8±3.1	72.9±2.2	75.5±1.0	77.5±1.2
F4	GeoCLR	SVM	H- k means	55.3±4.2	71.8±1.6	74.6±1.5	76.6±1.2	79.0±1.0
F5	GeoCLR	Res18	random	49.5±7.9	60.3±3.8	65.2±1.7	69.0±3.0	73.2±1.9
F6	GeoCLR	Res18	H- k means	56.5±3.4	65.5±1.4	66.8±1.9	70.9±1.3	73.9±1.7
F7	GeoCLR	Res18	PL-linear	64.2±2.5	71.7±2.3	72.7±1.6	73.5±1.4	75.7±1.6
F8	GeoCLR	Res18	PL-SVM	63.7±2.1	72.0±2.1	72.5±1.5	74.3±1.0	75.2±1.3

The same CNNs as Table 2 where different data selection strategies (*random* and *H-k means*) are used in the downstream classification task. In contrast to the *balanced* selection strategy shown in Table 2, these selection strategies do not require prior analysis by humans and so are available for analysis of data as they get collected in the field. The same classifiers (linear, SVM, fine-tuned ResNet18) are investigated. For fine-tuning the CNNs, pseudo-labels generated by linear classifier (*-7) or SVM (*-8) are used. The classifiers are trained 10 times with different random seed, and mean and SD values of f_1 scores (macro averaged) are shown. The best score for each M is shown as bold.

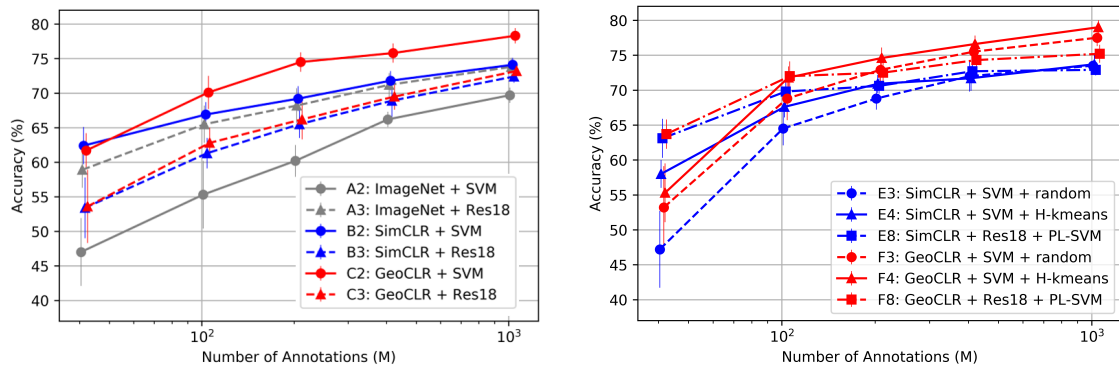
**(a)** CNN training method comparison for class-balanced training (Table 2)**(b)** Data selection method comparison for SimCLR and GeoCLR (Table 3)

Figure 5. Representative configurations from (a) Table 2 and (b) Table 3. (a) When the CNNs are trained on the class-balanced subsets, GeoCLR with a SVM classifier (C2) outperforms all other configurations except for B2 when $M = 40$. The best performance for $M = 40$ is achieved by GeoCLR with a linear classifier (C1). (b) In general, the use of *H-k means* improves performance compared to equivalent *random* configurations, and GeoCLR outperforms its counterparts with the SimCLR except for $\{M = 40, E4\}$.

strategies based on their location in the GeoCLR latent representations embedded by *t*-SNE (van der Maaten and Hinton, 2008). In this figure, $M = 30$ images are shown for ease of visualization, where the background points show the image representations that are not selected. The color of the points and selected image borders illustrate the human class annotation of each annotated image using the same color key as Figure 3. The visualization shows that *random* selection strategy fails to select images from the central region of the latent representation space that is relatively sparsely populated. On the other hand, *H-k means* selects images evenly from the different regions of the latent representation. When compared to the *balanced* selection strategy, it can be seen that there are several regions of the latent representation space that are not sampled. This is because they are mapped to different regions of the latent space as more densely populated regions that have the same class. These undersampled regions of the latent space can be easily confused by a classifier, where the final assigned class will depend on the distribution of nearby training samples.

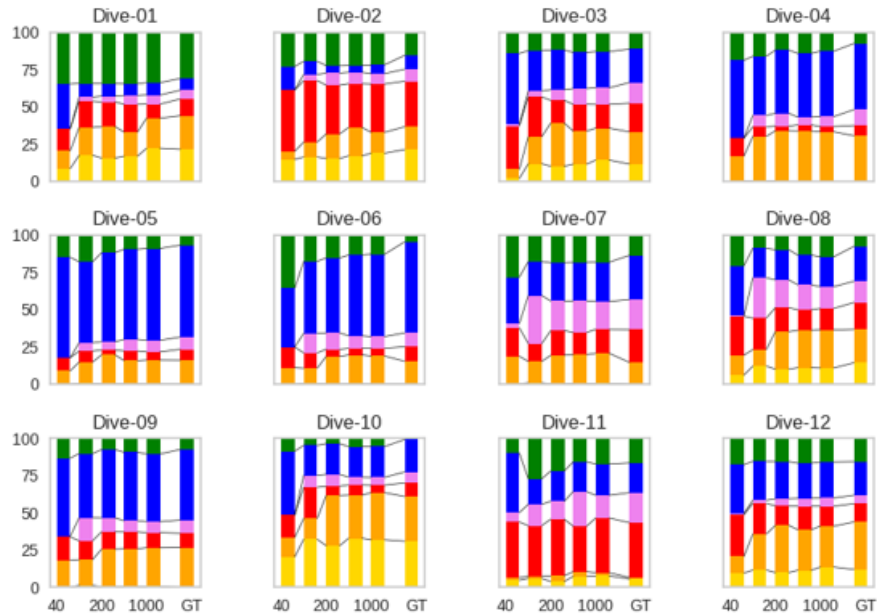
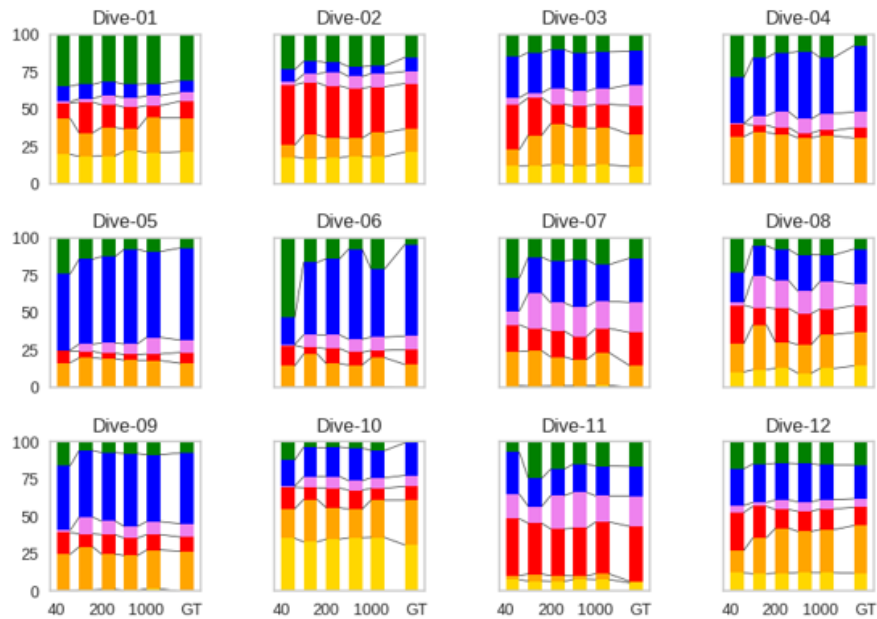
From a practical perspective, the proposed GeoCLR with $M = 100$ *H-k means* machine prioritized annotations and the SVM-RBF classifier (F4), and PL-SVM fine-tuning (F7) achieves the same accuracy as state-of-the-art transfer learning (i.e., D5, $M = 1000$) using an order-of-magnitude fewer human annotations. The method also achieves the same accuracy as state-of-the-art contrastive learning approaches (i.e., E3, $M = 400$) using a quarter of the annotations, where prior works rely on random data annotations and do not propose a data selection strategy. We consider being able to perform accurate classification with a relatively small number of labels (i.e., 0.1% of the entire dataset) an important development since providing 100 annotations represents a level of human effort that can be justified for most application in the field. We also show that for applications that can justify a larger amount of human effort (i.e., $M = 1000$), the proposed GeoCLR outperforms conventional transfer learning (D5) and contrastive learning (E3) by 8.5% and 7.5%, respectively. In addition to the demonstrated performance gains, the use of GeoCLR consistently improves performance over alternative configurations for all conditions tested in this work, and machine-guided annotation *H-k means* benefits performance for all configurations where $M < 400$, and although the performance gains diminish for larger M , it never leads to significant performance reduction. The results indicate that these approaches can robustly improve the performance of CNNs for seafloor image interpretation.

4.5. Applications

Determining seafloor habitat class distributions is a fundamental task for marine monitoring and conservation. Here we apply the proposed GeoCLR method to estimate the relative proportion of habitat classes and map their physical distribution.

4.5.1. Estimating Relative Habitat Class Proportion

Figure 6 shows the relative proportion of different habitat classes estimated for $M = [40, 100, 200, 400, 1000]$ machine-prioritized annotations for each of the 12 dives in the Tasmania dataset. These are compared to the relative proportions for each dive where all human annotations have been used (i.e., average 450 annotations per dive), which we consider to be the ground truth here. The equivalent number of annotations per dive for the proposed method average approximately 3 annotations per dive for $M = 40$ to approximately 83 per dive for $M = 1000$. The results show that the estimated proportions approach the ground truth distributions for all dives, with the expected result that performance increases as a larger number of annotations is used for classifier training. The estimated proportions are poor for several of the dives with $M = 40$ when using the F4 SVM classifier (Figure 6a), whereas the F8 fine-tuned with pseudo-labels generated by the SVM is generally more robust, approximating the ground truth class proportions better for the same number of training examples (Figure 6b). This indicates that the SVM classifier (F4) may be overfitting the latent representation space generated by GeoCLR when the number of annotations available is small, where this effect is mitigated by providing a larger number of training examples through pseudo-labels. However, there are some exceptions (dives 06 and 07) to this and so the

(a) F4 in Table 2 (SVM on latent representation h)

(b) F8 in Table 2 (fine-tuned on pseudo-labels generated by SVM)

Figure 6. Class distribution estimated for each dive based on the proposed GeoCLR. The same color scheme is used as in Figure 3. The estimated distributions approach the ground truths when a larger number of annotations is used for classifier training. The use of pseudo-labels is generally favorable for a small number of annotations (i.e., $M = 40$), though this is not always the case. For $M > 100$, F4 performs better than F8 and provides more stable estimates of class distribution as the same latent representation space is used for all M .

outputs with $M = 40$ should be treated with caution where validation data are not available. On the other hand, for $M \geq 100$ both methods (i.e., F4 and F8) perform robustly for all dives, with F4 outperforming F8 and providing more stable estimates for different values of M . This is due to the fact that the latent representation space remains the same regardless of M as no CNN re-training takes place.

4.5.2. Habitat Mapping

The physical distribution of habitats is important for conservation since it influences the distribution of organisms near the seafloor. It is also important for understanding ecosystem health as benthic habitats such as kelp (seen here) and coral are classified as essential ocean variables.

The proposed method allows efficient estimation of habitat maps based on the 3D location where each classified image was taken. Here, we show the horizontal distributions of the classes, the depth profiles vs. image index, and the class vs. depth distributions in Figures 7, 8, and 9 for three dives (01, 03, and 08) which were chosen as representative cases. The figures show habitat maps generated using GeoCLR for $\{M = 100, F8\}$, $\{M = 1000, F4\}$ in Table 3 and the ground truth labels.

The results show that both $\{M = 100, F8\}$ and $\{M = 1000, F4\}$ configurations closely approximate the ground truth horizontal and vertical habitat class distributions, capturing the continuous

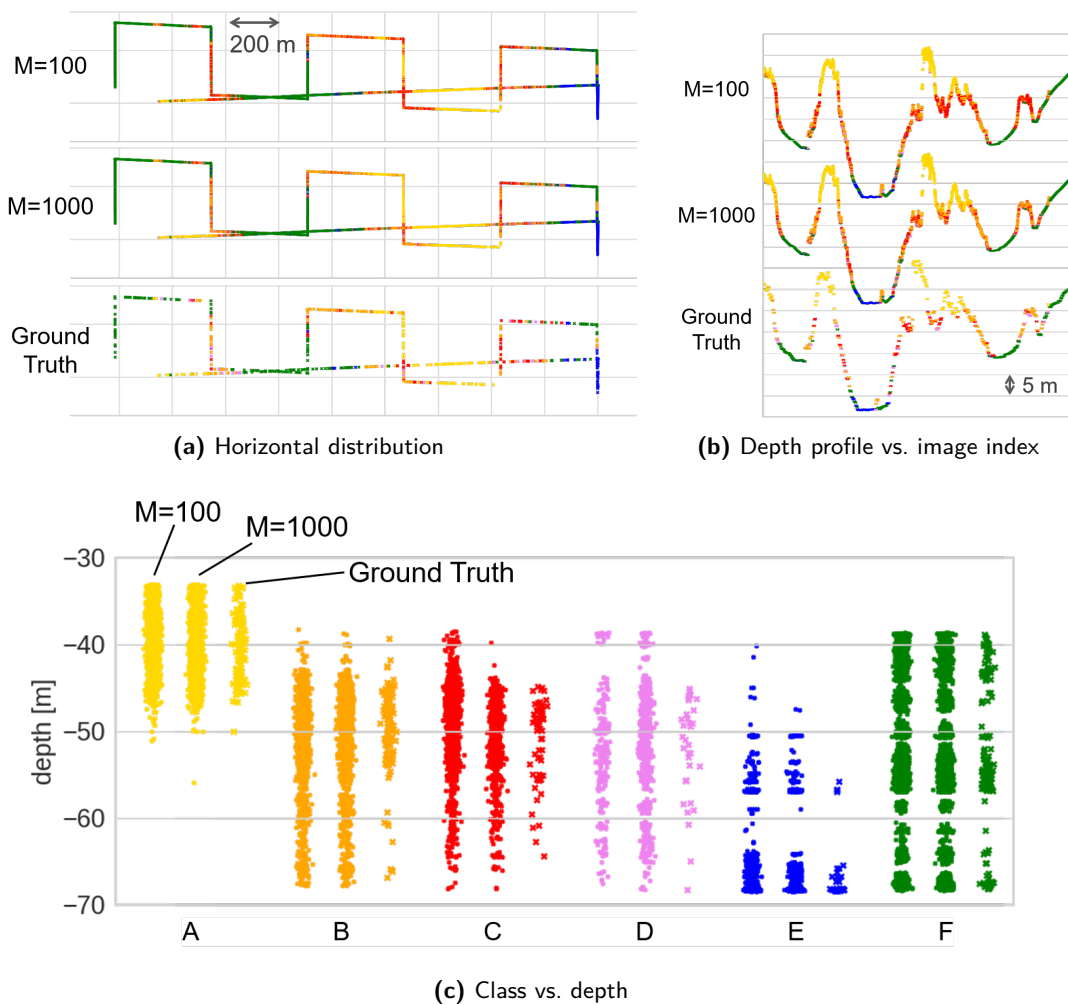


Figure 7. Class distribution of dive 01 with $M = 100$ annotations by F8, $M = 1000$ annotations by F4 in Table 3 and ground truth. The same color scheme as Figure 3 is applied.

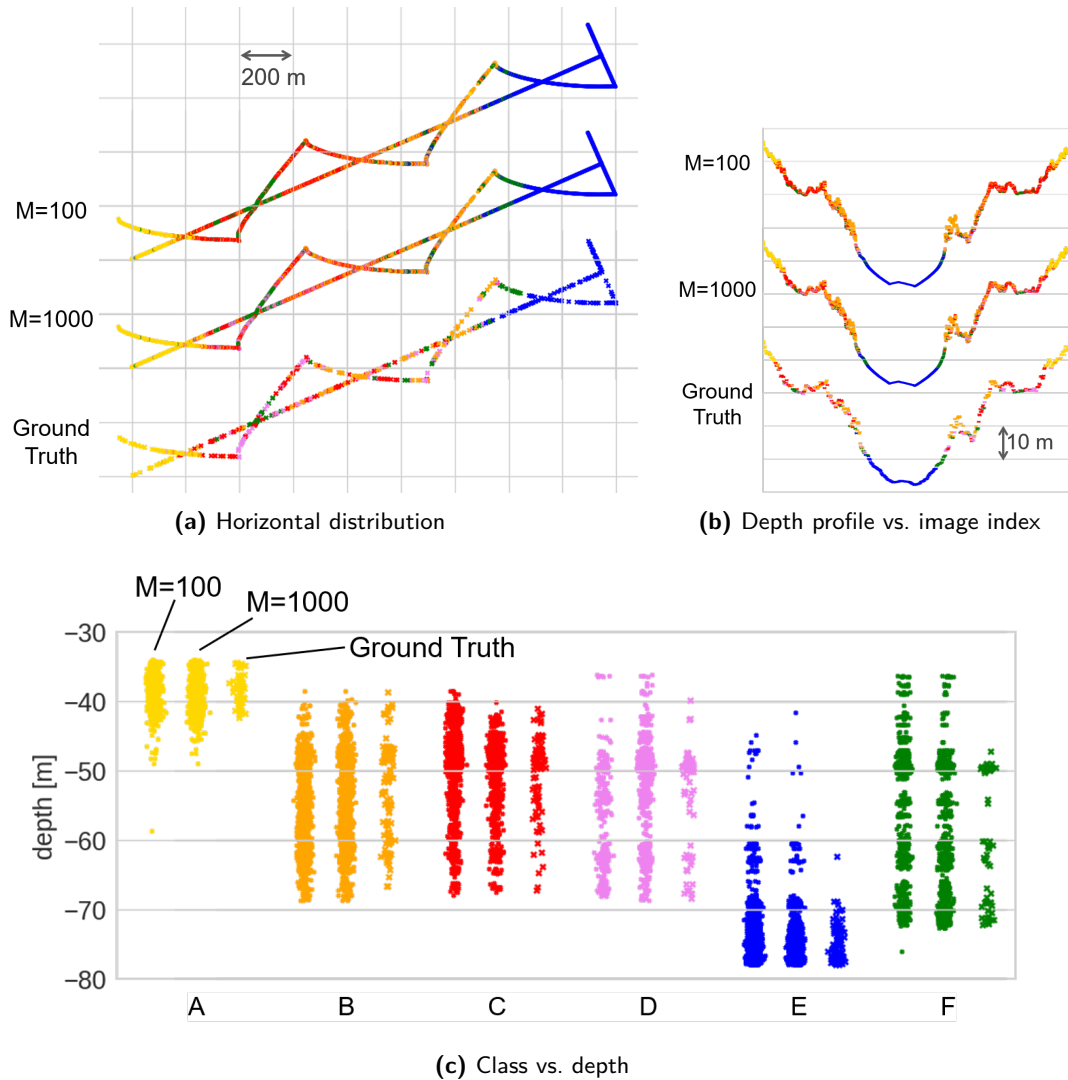


Figure 8. Class distribution of dive 03 with $M = 100$ annotations by F8, $M = 1000$ annotations by F4 in Table 3 and ground truth. The same color scheme as Figure 3 is applied.

spatial transitions between kelp (A), low relief reef (C), high relief reef (B) to screw shell rubble (E) or sand (F). The class vs. depth distributions show that the larger values of M provide a better approximation of vertical class distribution, which is an expected result. However, for classes that exist in a limited depth band (e.g., kelp (A), screw shell rubble (E)), both values of M capture this trend.

5. Conclusion

The paper has developed a method to use georeferenced information in contrastive learning for efficient training of deep-learning CNNs. The proposed georeference contrastive learning for seafloor image representation (GeoCLR) method is effective for datasets where the targets of interest for semantic interpretation are distributed over spatial scales larger than the footprint of a single image frame. The underlying assumption is that images gathered within a close distance are more likely to have similar visual appearance than images that are taken far apart. This assumption can be

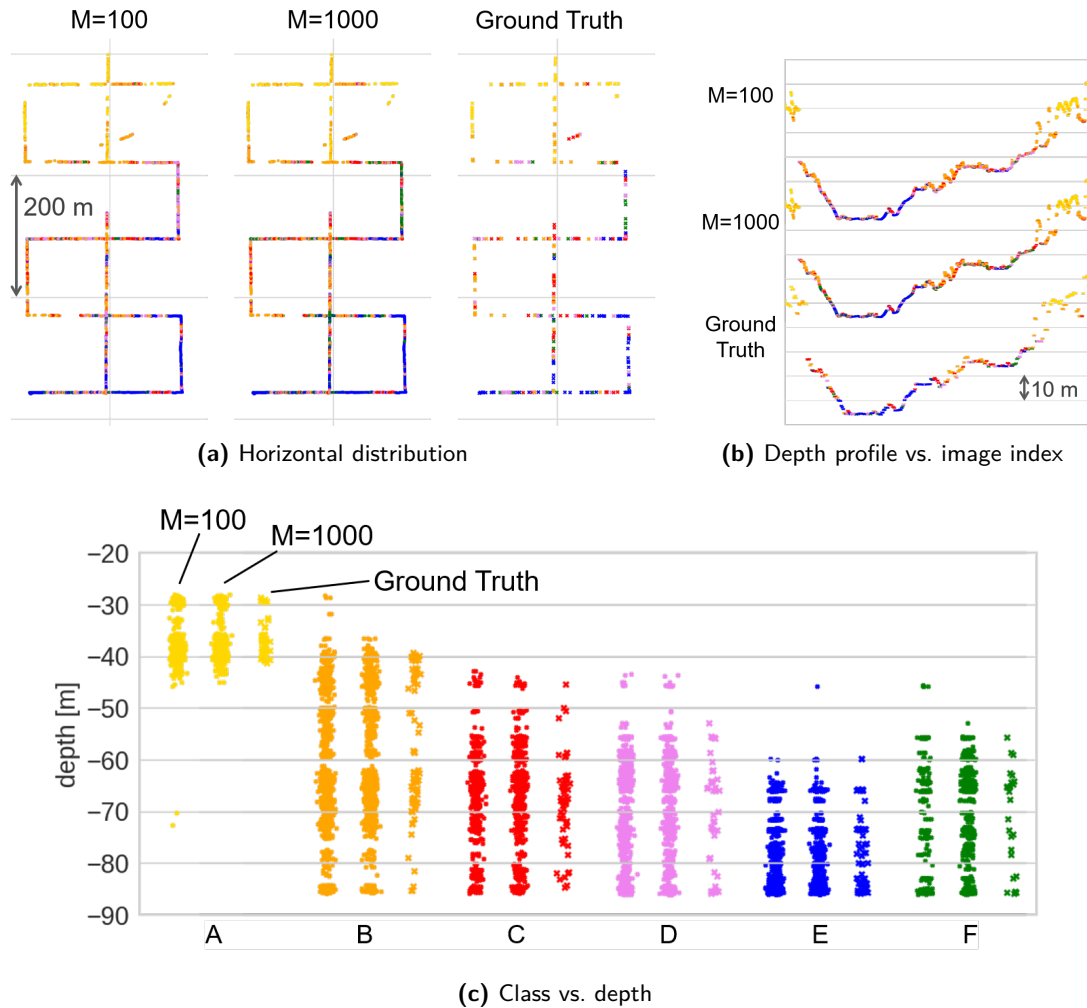


Figure 9. Class distribution of dive 08 with $M = 100$ annotations by F8, $M = 1000$ annotations by F4 in Table 3 and ground truth. The same color scheme as Figure 3 is applied.

reasonably satisfied in seafloor robotic imaging applications, where (1) images are acquired at close and regular intervals along a vehicle's trajectory, and (2) the targets for interpretation are substrates and habitats which typically have extents much greater than the image footprint. The method can be deployed on any CNN, and performance gains can be achieved without any prior human input to interpret the dataset. We demonstrate the performance of the proposed training method using a CNN architecture that can be deployed on computers that can be reasonably expected to be available during a field survey, without relying on network access to supercomputers, and can generate results in timeframes that are relevant for ongoing field expeditions. Experiments on a robotically obtained seafloor image dataset that includes more than $\sim 86,000$ images and $\sim 5,000$ annotations show that

- The proposed GeoCLR method outperforms existing state-of-the-art contrastive learning (SimCLR) and transfer learning for downstream supervised classification tasks using an equivalent CNN architecture (ResNet18). On an ideal, class-balanced training dataset, the SVM with RBF kernel trained on the features extracted by the GeoCLR trained CNN shows an average of 5.2% and maximum of 7.7% improvement compared to the accuracy scores of SimCLR for $M = [40, 100, 200, 400, 1000]$ annotations. Compared to ResNet18 trained by transfer learning, an average improvement of 7.4% and a maximum of 9.2% are achieved.

- The representations extracted by the GeoCLR are useful for identifying representative images for prioritized human annotation in a fully unsupervised manner. This can improve the performance and efficiency of human effort for classification, where selecting a prioritized training dataset using H - k -means clustering increases the classification accuracy by an average of 4.9% and maximum of 14.1% compared to random selection, where the performance gains are more significant for small numbers of M . Compared with SimCLR, GeoCLR latent representations show 7.1% better score on average with randomly annotated $M = [40, 100, 200, 400, 1000]$ training datasets. Prioritized annotating by H - k means allows score improvements for all M values, leading to 10.2% increase in total.
- Selecting representative images for prioritized labeling based on their distribution in the GeoCLR latent representation space results in better performance than providing class-balanced annotated examples. The machine-driven H - k -means selection strategy achieves an average of 1.6% and maximum of 3.1% increase in accuracy compared to the class-balanced selection strategy for an equivalent number of annotations, where greater gains are achieved for small numbers of annotations. This indicates that it is more informative to provide training data that evenly describe the latent representation space generated during self-supervised training than it is to provide training data that evenly describe the targets that are of final interest to humans.
- The combination of GeoCLR and H - k means achieves the same accuracy as state-of-the-art transfer learning using an order-of-magnitude fewer human annotations, and state-of-the-art contrastive learning approaches using a quarter of the labels. This allows the proportion of habitat classes and their spatial distribution to be accurately estimated ($> 70\%$) annotating only 0.1% of the images in the dataset. This is significant as providing approximately 100 annotations represents a level of human effort that can be justified for most field applications. For applications where a greater level of human effort is available, we show that with 1,000 annotations, the proposed GeoCLR outperforms conventional transfer learning and contrastive learning by 8.5% and 7.5%, respectively, achieving a classification accuracy of 79%. The combination of GeoCLR and H - k means never degraded performance compared to equivalent alternative configurations in the experiments described in this paper.

Acknowledgments

This work was carried out under the UK Natural Environment Research Council's Oceanids Biocam project NE/P020887/1 and Australian Research Council's Automated Benthic Understanding DP190103914 Discovery project.

ORCID

Takaki Yamada  <https://orcid.org/0000-0002-5090-7239>

Adam Prügel-Bennett  <https://orcid.org/0000-0002-1329-5077>

Stefan B. Williams  <https://orcid.org/0000-0001-9416-5639>

Oscar Pizarro  <https://orcid.org/0000-0001-6612-2738>

Blair Thornton  <https://orcid.org/0000-0003-4492-622X>

References

- Beijbom, O., Edmunds, P. J., Kline, D. I., Mitchell, B. G., and Kriegman, D. (2012). Automated annotation of coral reef survey images. In *2012 IEEE Conference on Computer Vision and Pattern Recognition*, pages 1170–1177. IEEE.
- Bewley, M., Nourani-Vatani, N., Rao, D., Douillard, B., Pizarro, O., and Williams, S. B. (2015). Hierarchical classification in AUV imagery. In *Field and Service Robotics*, pages 3–16. Springer.
- Chen, T., Kornblith, S., Norouzi, M., and Hinton, G. (2020). A simple framework for contrastive learning of visual representations. In *International Conference on Machine Learning*, pages 1597–1607. PMLR.

- Deng, J., Dong, W., Socher, R., Li, L.-J., Li, K., and Fei-Fei, L. (2009). Imagenet: A large-scale hierarchical image database. In *2009 IEEE Conference on Computer Vision and Pattern Recognition*, pages 248–255. IEEE.
- Goyal, P., Dollár, P., Girshick, R., Noordhuis, P., Wesolowski, L., Kyrola, A., Tulloch, A., Jia, Y., and He, K. (2017). Accurate, large minibatch SGD: Training ImageNet in 1 hour. *arXiv preprint arXiv:1706.02677*.
- He, K., Zhang, X., Ren, S., and Sun, J. (2016). Deep residual learning for image recognition. In *Proceedings of the IEEE Conference on Computer Vision and Pattern Recognition*, pages 770–778. IEEE.
- Jing, L., and Tian, Y. (2021). Self-supervised visual feature learning with deep neural networks: A survey. *IEEE Transactions on Pattern Analysis and Machine Intelligence*, 43(11):4037–4058. doi: 10.1109/TPAMI.2020.2992393.
- Johnson-Roberson, M., Pizarro, O., Williams, S. B., and Mahon, I. (2010). Generation and visualization of large-scale three-dimensional reconstructions from underwater robotic surveys. *Journal of Field Robotics*, 27(1):21–51.
- Kaeli, J. W., and Singh, H. (2015). Online data summaries for semantic mapping and anomaly detection with autonomous underwater vehicles. In *OCEANS 2015-Genova*, pages 1–7. IEEE.
- Krizhevsky, A., Sutskever, I., and Hinton, G. E. (2012). ImageNet classification with deep convolutional neural networks. In *Advances in Neural Information Processing Systems*, pages 1097–1105.
- Le-Khac, P. H., Healy, G., and Smeaton, A. F. (2020). Contrastive representation learning: A framework and review. *IEEE Access*.
- Mahmood, A., Bennamoun, M., An, S., Sohel, F. A., Boussaid, F., Hovey, R., Kendrick, G. A., and Fisher, R. B. (2018). Deep image representations for coral image classification. *IEEE Journal of Oceanic Engineering*, 44(1):121–131.
- Mahon, I., Williams, S. B., Pizarro, O., and Johnson-Roberson, M. (2008). Efficient view-based SLAM using visual loop closures. *IEEE Transactions on Robotics*, 24(5):1002–1014.
- Moltmann, T., Turton, J., Zhang, H.-M., Nolan, G., Gouldman, C., Griesbauer, L., Willis, Z., Piniella, A. M., Barrell, S., Andersson, E., Gallage, C., Charpentier, E., Belbeoch, M., Poli, P., Rea, A., Burger, E. F., Legler, D. M., Lumpkin, R., Meinig, C., O’Brien, K., Saha, K., Sutton, A., Zhang, D., and Zhang, Y. (2019). A global ocean observing system (GOOS), delivered through enhanced collaboration across regions, communities, and new technologies. *Frontiers in Marine Science*, 6:291.
- Neettiyath, U., Thornton, B., Sangekar, M., Nishida, Y., Ishii, K., Bodenmann, A., Sato, T., Ura, T., and Asada, A. (2021). Deep-sea robotic survey and data processing methods for regional-scale estimation of manganese crust distribution. *IEEE Journal of Oceanic Engineering*, 46(1):102–114. doi: 10.1109/JOE.2020.2978967.
- Nister, D., and Stewenius, H. (2006). Scalable recognition with a vocabulary tree. In *2006 IEEE Computer Society Conference on Computer Vision and Pattern Recognition (CVPR’06)*, volume 2, pages 2161–2168. IEEE.
- Ojala, T., Pietikäinen, M., and Mäenpää, T. (2002). Multiresolution gray-scale and rotation invariant texture classification with local binary patterns. *IEEE Transactions on Pattern Analysis & Machine Intelligence*, (7):971–987.
- Rao, D., De Deuge, M., Nourani-Vatani, N., Williams, S. B., and Pizarro, O. (2017). Multimodal learning and inference from visual and remotely sensed data. *International Journal of Robotics Research*, 36(1):24–43.
- Satopaa, V., Albrecht, J., Irwin, D., and Raghavan, B. (2011). Finding a “kneedle” in a haystack: Detecting knee points in system behavior. In *2011 31st International Conference on Distributed Computing Systems Workshops*, pages 166–171. IEEE.
- Sohn, K. (2016). Improved deep metric learning with multi-class n-pair loss objective. In *Proceedings of the 30th International Conference on Neural Information Processing Systems*, pages 1857–1865.
- Steinberg, D., Friedman, A., Pizarro, O., and Williams, S. B. (2011). A Bayesian nonparametric approach to clustering data from underwater robotic surveys. In *International Symposium on Robotics Research*, volume 28, pages 1–16.
- Tan, C., Sun, F., Kong, T., Zhang, W., Yang, C., and Liu, C. (2018). A survey on deep transfer learning. In *International Conference on Artificial Neural Networks*, pages 270–279. Springer.
- van den Oord, A., Li, Y., and Vinyals, O. (2018). Representation learning with contrastive predictive coding. *arXiv preprint arXiv:1807.03748*.
- van der Maaten, L., and Hinton, G. (2008). Visualizing data using t-SNE. *Journal of Machine Learning Research*, 9(November):2579–2605.

- Williams, S. B., Pizarro, O. R., Jakuba, M. V., Johnson, C. R., Barrett, N. S., Babcock, R. C., Kendrick, G. A., Steinberg, P. D., Heyward, A. J., Doherty, P. J., Mahon, I., Johnson-Roberson, M., Steinberg, D., and Friedman, A. (2012). Monitoring of benthic reference sites: Using an autonomous underwater vehicle. *IEEE Robotics Automation Magazine*, 19(1):73–84.
- Wu, Z., Xiong, Y., Yu, S. X., and Lin, D. (2018). Unsupervised feature learning via non-parametric instance discrimination. In *Proceedings of the IEEE Conference on Computer Vision and Pattern Recognition*, pages 3733–3742. IEEE.
- Yamada, T., Massot-Campos, M., Prügel-Bennett, A., Pizarro, O., Williams, S., and Thornton, B. (2022). Guiding labelling effort for efficient learning with georeferenced images. *IEEE Transactions on Pattern Analysis and Machine Intelligence*, Early Access.
- Yamada, T., Massot-Campos, M., Prügel-Bennett, A., Williams, S. B., Pizarro, O., and Thornton, B. (2021a). Leveraging metadata in representation learning with georeferenced seafloor imagery. *IEEE Robotics and Automation Letters*, 6(4):7815–7822.
- Yamada, T., Prügel-Bennett, A., and Thornton, B. (2021b). Learning features from georeferenced seafloor imagery with location guided autoencoders. *Journal of Field Robotics*, 38(1):52–67.
- Yang, J., Yu, K., Gong, Y., and Huang, T. (2009). Linear spatial pyramid matching using sparse coding for image classification. In *2009 IEEE Conference on Computer Vision and Pattern Recognition*, pages 1794–1801. IEEE.

How to cite this article: Yamada, T., Prügel-Bennett, A., Williams, S. B., Pizarro, O., & Thornton, B. (2022). GeoCLR: Georeference contrastive learning for efficient seafloor image interpretation. *Field Robotics*, 2, 1134–1155.

Publisher’s Note: Field Robotics does not accept any legal responsibility for errors, omissions or claims and does not provide any warranty, express or implied, with respect to information published in this article.

Appendix: Sensitivity to hyperparameters

The main contribution of the GeoCLR method is that selecting similar image pairs that are physically close to each other will provide a better representation of variability in contrastive learning than traditional data augmentation.

The conditions for a pair of images to be physically close enough is determined by the following equation (Eq. (3) in the main text):

$$\sqrt{(g'_{east} - g_{east})^2 + (g'_{north} - g_{north})^2 + \lambda(g'_{depth} - g_{depth})^2} \leq r, \quad (3)$$

where $(g_{east}, g_{north}, g_{depth})$ is the 3D georeference of image \mathbf{x} . Equation (3) includes two hyperparameters: r , which corresponds to a 3D distance threshold where images captured within this range are regarded as similar, and λ , which is a weight for the depth difference between images. These hyperparameters relate to the physical characteristics of observed seafloor habitats and substrates, and so their optimized values are considered to be dataset dependent. This Appendix investigates the sensitivity of learning performance to these hyperparameters for the Tasmania dataset considered in this work.

Table A1 shows the f_1 scores of linear classifiers trained on the obtained latent representations for different r values ($r = 0.0, 1.0, 3.0, 5.0, 10.0$ m) for fixed $\lambda = 1.0$. Class balanced training datasets with different numbers of images ($M = 40, 100, 200, 400, 1000$) have been used to train the classifier, which is the same configuration as B1 (for $r = 0.0$ m) or C1 (others) in Table 2 of the main paper. The best performance is using $r = 1.0$ m for all M , showing that it is optimal for this dataset. Since the AUV traveled at 0.5 m/s with image acquisition at 1 fps, $r = 1.0$ m is the smallest value where most images will have at least two nearby images to form a similar pair for contrastive learning. Larger r values will have more images to choose from for the similar pair, but as the distances between the pair increases, we expect their appearances to become less similar. If r is too small, there will be no nearby images to select from, and so only augmentation on the same image can be performed (i.e., the same as SimCLR). The latent representations obtained with the larger r values ($r = 3.0, 5.0, 10.0$ m) show poorer performance scores than $r = 1.0$ m for all M . However, they still perform better than the original SimCLR ($r = 0.0$ m) except for a few cases with $M = 40, 100$. It can be assumed that the optimal r value depends on the habitat and substrate patch sizes in the observed area. Even if the size of these semantic patches is not known, we can expect smaller r values to perform robustly since similar appearance image pairs are likely to be sampled, compared with larger r , under the assumption that semantic patches of interest for habitat and substrate mapping occur on spatial scales larger than the footprint of a single image frame.

Table A2 shows the f_1 scores trained on the latent representations obtained using the optimal r value ($r = 1.0$ m) with the different λ values ($\lambda = 0.0, 0.5, 3.0, 5.0, 10.0$) for the Tasmania dataset. Increasing λ increases sensitivity to depth differences, making it more likely for a potential similar pair to be rejected if there is a difference in their depths. Though the scores differ slightly depending on the λ values, their standard deviation values show these differences within the margin of error.

Table A1. Performance sensitivity to hyperparameter r (in meters) when validated on class-balanced training subsets

r	Number of Annotations (M)				
	40	100	200	400	1000
0.0 (SimCLR)	62.5 ± 2.7	65.2 ± 2.8	67.1 ± 1.2	69.2 ± 2.2	71.8 ± 1.0
1.0	63.8 ± 2.9	67.8 ± 2.4	71.4 ± 1.4	72.9 ± 1.8	74.9 ± 1.0
3.0	59.7 ± 2.7	64.4 ± 2.4	69.2 ± 3.4	70.8 ± 2.1	72.8 ± 1.4
5.0	61.1 ± 2.2	65.9 ± 2.4	68.4 ± 1.6	71.1 ± 1.8	71.9 ± 2.3
10.0	60.5 ± 2.5	66.1 ± 3.0	68.5 ± 2.5	70.5 ± 3.1	72.9 ± 1.7

$r = 0.0$ is equivalent to SimCLR (B1 in Table 2).

Table A2. Performance sensitivity to hyperparameter λ when validated on class-balanced training subsets

λ	Number of Annotations (M)				
	40	100	200	400	1000
0.0	63.8 ± 3.3	69.2 ± 2.9	72.5 ± 1.7	74.0 ± 1.9	75.6 ± 1.3
0.5	63.7 ± 4.7	68.4 ± 3.1	71.8 ± 2.0	74.0 ± 1.9	76.6 ± 2.1
1.0	63.8 ± 2.9	67.8 ± 2.4	71.4 ± 1.4	72.9 ± 1.8	74.9 ± 1.0
3.0	65.3 ± 4.6	70.2 ± 2.9	72.7 ± 2.9	74.4 ± 1.7	75.9 ± 1.3
5.0	63.8 ± 2.6	69.6 ± 3.4	72.3 ± 2.3	74.2 ± 1.7	75.3 ± 1.7
10.0	64.0 ± 3.7	68.7 ± 3.3	72.9 ± 2.0	74.3 ± 2.5	76.0 ± 1.6

The reason why λ is less sensitive to the performance than r can be considered that rugosity and slope in the Tasmania dataset are relatively small. For the datasets with more drastic depth changes we expect greater sensitivity to λ values.